HHS Public Access

Author manuscript

Nat Cell Biol. Author manuscript; available in PMC 2011 December 01.

Published in final edited form as:

Nat Cell Biol. 2011 June ; 13(6): 641–651. doi:10.1038/ncb2233.

Basement Membrane Sliding and Targeted Adhesion Remodels Tissue Boundaries During Uterine-vulval Attachment in *C. elegans*

Shinji Ihara[1], **Elliott J. Hagedorn**[1], **Meghan A. Morrissey**[1], **Qiuyi Chi**[1], **Fumio Motegi**[2], **James M. Kramer**[3], and **David R. Sherwood**[1]

[1]Department of Biology, Duke University, Science Drive, Box 90388, Durham, NC 27708 USA

[2]Department of Molecular Biology and Genetics, Howard Hughes Medical Institute, Center for Cell Dynamics, Johns Hopkins School of Medicine, Baltimore, MD 21205, USA

[3]Department of Cell and Molecular Biology, Northwestern University Medical School, Chicago, IL 60611, USA

Abstract

Large gaps in basement membrane (BM) occur at sites of cell invasion and tissue remodelling in development and cancer. Though never followed directly *in vivo*, BM dissolution or reduced synthesis have been postulated to create these gaps. Using landmark photobleaching and optical highlighting of laminin and type IV collagen, we find that a new mechanism, BM sliding, underlies BM gap enlargement during uterine-vulval attachment in *C. elegans*. Laser ablation and mutant analysis reveal that the invaginating vulval cells promote BM movement. Further, an RNA interference and expression screen identify the integrin INA-1/PAT-3 and VAB-19, homolog of the tumour suppressor Kank, as regulators of BM opening. Both concentrate within vulval cells at the BM gap boundary and halt expansion of the shifting BM. BM sliding followed by targeted adhesion represents a new mechanism for creating precise BM breaches that can be used by cells to break down compartment boundaries.

INTRODUCTION

Cells navigate complex networks of extracellular matrix during many developmental, physiological and pathogenic processes [1,2]. One of the main matrix barriers cells encounter is basement membrane (BM), a thin, dense, sheet-like structure built on a network of polymeric laminin and type IV collagen. BMs are ubiquitous in multicellular animals, enveloping most tissues and providing the structural underpinning for all epithelia and

*Correspondence: David Sherwood[1] (david.sherwood@duke.edu).

CONTRIBUTIONS

S.I. carried out most of the experiments. All other authors performed particular subsets of experiments or developed key reagents. D.R.S and S.I designed the project and D.R.S., S.I., E.J.H. and M.A.M. wrote the manuscript.

Supplementary Information

Supplementary Information includes five figures, five tables and five movies.

endothelia [3]. Cell-BM interactions have been difficult to experimentally examine *in vivo* and problematic to recapitulate *in vitro*, owing to the complexities of native BM structure and cellular environment [4–6]. Thus, the mechanisms cells use to remodel BM barriers remain poorly understood.

De novo gaps in BM form during developmental processes such as gastrulation and organogenesis, and facilitate tissue remodelling and cell movement [7–9]. Metastatic tumours are thought to use the same molecular programs to create gaps to enable their spread [5,10–14]. The expression of matrix-degrading proteases and the presence of type IV collagen degradation products surrounding and within invasive cells has led to the idea that BM barriers are overcome through proteolytic degradation [15–22]. Based in part on these observations, inhibitors of matrix metalloproteinases have been used in clinical trials for patients with advanced cancer, though patient survival was not increased [18]. Reduced BM synthesis and changes in composition have also been postulated to underlie localized loss [11,14,23]. To resolve the mechanisms that cells use to overcome BM barriers it is crucial to follow the fate of breached BM *in vivo* and experimentally examine the removal mechanisms.

Anchor cell (AC) invasion into the vulval epithelium in *C. elegans* is an experimentally and visually accessible model of invasion through BM [8]. The AC is a specialized gonadal cell that breaches the juxtaposed gonadal and ventral epidermal BMs, and contacts the central 1° fated vulval precursor cells to initiate uterine-vulval attachment. After AC invasion, neighbouring uterine and vulval cells attach to complete uterine-vulval connection [24]. The fate of the BM during these later phases of attachment is unknown.

Utilizing cell- and BM-specific markers we report here that the breach in the BM widens dramatically during the later stages of uterine-vulval attachment. Landmark photobleaching and optical marking of laminin and type IV collagen reveal that neither reduced BM deposition nor dissolution account for BM gap expansion. Instead, we show that the BM breach is widened through BM sliding, and that this shift is dependent on the invaginating vulval cells. Further, we find that the integrin heterodimer INA-1/PAT-3, and VAB-19, the *C. elegans* homolog of the tumour suppressor protein Kank [25,26], localize within the vulval cells at the BM gap boundary and halt BM sliding. These studies reveal a new mechanism to widen and stabilize BM breaches during tissue remodelling.

RESULTS

Summary of Uterine-vulval Attachment

During the mid L3 larval stage, the ventral uterine (VU) and vulval precursor cells (VPCs, P5.p-P7.p cell daughters) are separated by the juxtaposed gonadal and ventral epidermal basement membranes (BMs; Figure 1A). During the mid-to-late L3 larval stage, a specialized uterine cell, the anchor cell (AC), initiates uterine-vulval attachment by invading through both BMs and contacting the underlying descendants of the 1°-fated daughters of the VPC P6.p (P6.p four-cell stage) [8]. Following invasion, the underlying vulval cells divide and invaginate. By the early L4 stage, the AC fuses with neighbouring ventral uterine cells and forms the multinucleated utse cell, which together with the ventral uterine uv1 cells

contact the 1°-fated great-granddaughters of P6.p, completing the direct connection between the uterine and vulval tissues [24,27,28]. The vulD cells (inner most granddaughters of the 2°-fated VPCs, P5.p and P7.p) and the uv2, uv3 (descendants of dorsal uterine (DU) cells) and ut cells (descendants of ventral uterine (VU) cells) sit adjacent to the connection on the vulval and uterine sides, respectively (Figure 1A). During these later stages of uterine-vulval attachment, the fate and dynamics of the BM is unknown.

The Breach in the BM Expands and Stabilizes over the vulD Cells

To examine BM localization during uterine-vulval attachment we used a functional translational fusion of the lone laminin β subunit to GFP (*laminin::GFP*), which shows identical expression to immunolocalized laminin [8,29]. The AC plasma membrane was viewed using the pleckstrin-homology (PH) domain from phospholipase C-δ fused to mCherry and driven by an AC-specific promoter (*cdh-3 > mCherry::PLCδ^{PH}*) [30]. During the time of AC invasion (P6.p four-cell stage), the AC remained in direct contact with the BM breach, which was positioned over the central P6.p granddaughters (Figure 1B and 1C; Movies S1 and S2). Separation of the uterine and vulval tissues' tightly juxtaposed BMs revealed that they became fused at the borders of the invading AC and formed a continuous BM throughout uterine-vulval attachment (Figure 1G). When the vulval cells initiated invagination, the initial breach in the BM widened to extend over the outer P6.p granddaughters and expanded beyond the AC plasma membrane (Figure 1D and 1H; Movie S3). This expansion continued during the early P6.p eight-cell stage and then stabilized over the vulD cells (Figure 1E; Movie S4), a position directly abutting the multinucleate uterine utse cell in the mid L4 stage (Figure 1F and 1H). Transgenic animals expressing the BM components SPARC (*sparc::GFP*) and the sole *C. elegans* α1-like type IV collagen chain (*type IV collagen::mCherry*) [31,32], showed identical BM gap positioning. Thus, the breach in the BM widens beyond the AC and stabilizes over the vulD cells at the L4 stage during uterine-vulval attachment.

The AC Initiates but does not Complete BM Gap Formation

To determine if the AC has a role in widening the BM breach, we laser-ablated the AC at time points prior to and after invasion and examined laminin::GFP (Figure 2A and 2B). When the AC was ablated just prior to invasion, the BM remained completely intact through the L4 stage (Figure 2A; 16/16 animals examined). Blocking invasion in animals expressing a dominant negative form of the *C. elegans* integrin specifically in the AC (*zmp-1 > HA-βtail*) [33] also resulted in a failure to generate BM gap (20/20 animals). In contrast, BM gap expansion was normal when the AC was killed just after invasion (19/19 animals; Figure 2B). We conclude that the AC is required to initiate a breach in the BM, but dispensable for BM gap expansion.

The Descendants of the Ventral Uterine Cells Limit BM Gap Opening

The AC ablation experiments suggested that neighbouring uterine or vulval cells regulate BM gap opening once the AC makes the initial breach. To investigate a possible role for the uterine cells, we first laser ablated the dorsal uterine cells [34]. Removal of the dorsal uterine cells and their descendants did not alter the expansion or positioning of the BM gap (Table

1; Figure 2C). In contrast, laser ablation of the ventral uterine cells perturbed gap formation. Surprisingly, this alteration resulted in BM gap boundaries over-expanding in nearly 20% of operated animals (moving beyond the vulD cell; the remaining animals had normal BM gap positioning; Table 1; Figure 2D). Thus, the ventral uterine cell descendants restrict BM gap expansion.

The Vulval Cells Promote BM Gap Expansion

To determine if the vulval cells play a role in promoting BM gap expansion, we first examined BM opening in vulvaless animals (genotype *lin-3(n1059)/lin-3(n378)*) [35], a condition where approximately 20% of ACs invade [8]. In these cases, we found that the BM gap never extended beyond the AC (n = 10/10 animals; Figure 3A, 3B and 3E; Movie S5). Similar results were observed in animals where vulval cell divisions were blocked with hydroxyurea (n = 10/10 animals; Figure 3C and 3E) [8]. To further examine the role of the vulval cells in promoting BM gap expansion, we reduced the number of VPCs by laser ablating all VPCs except the innermost P6.p descendants P6.pa and P6.pp, a treatment that does not interfere with AC invasion and results in the isolated development of 1° fated vulF cells (see Figure 1A). This reduction of the number and invagination of VPCs decreased the expansion of the BM gap (Figure 3D and 3E). These results indicate that the vulval cells promote BM gap expansion. Furthermore, the degree of BM gap enlargement appears tied to vulval cell division or invagination.

BM Sliding Underlies Gap Expansion

Breaches in BM that form during developmental processes and in tumorigenesis have been postulated to result from proteolytic dissolution or reduced BM deposition [5]. To determine if proteolytic degradation underlies gap expansion, we first conducted an RNAi screen, examining BM gap expansion after RNAi mediated knockdown of 260 of the 298 *C. elegans* genes with putative protease or protease inhibitor domains (Table S1). No defects in BM gap expansion, however, were observed (Table S2). To further test a role for BM dissolution, we established transgenic worms expressing laminin::Dendra and type IV collagen::Dendra. Dendra is a highly-stable, photoconvertible fluorescent protein that changes from the green to red fluorescent state using low-phototoxic short wavelength light [36]. We converted a 5μm wide segment of BM at the edge of the forming gap at the P6.p four-cell stage (Figure 4A; Figure S1) and followed this highlighted boundary BM until the P6.p eight-cell stage. If dissolution accounted for gap expansion, we predicted that the optically highlighted boundary BM would be removed. Instead, we found the highlighted BM was not lost, but rather shifted from a location over the 1° fated vulF cells to a position above the 2° fated vulD cells (Figure 4A; n = 33/33 animals examined). Measurements of the photoconverted BM confirmed it did not shrink during movement, but did slightly expand, possibly a result of laminin diffusion or the gonadal and ventral epidermal BMs shifting relative to each other (Figure 4C). Notably, photoconversion of a small (approximately 1.25μm) region of laminin::Dendra at the BM boundary never visibly separated during sliding (n = 5/5 animals), suggesting that the two BMs slid in register. We observed a decrease in fluorescence of the photoconverted laminin::Dendra, however, this was comparable to control regions and likely a result of photobleaching and BM turnover (Figure 4D). Similar

results were obtained with type IV collagen::Dendra, suggesting that sliding is a property of this region of BM (Supplementary Information, Figure S1).

To determine if reduced BM deposition might also contribute to BM gap expansion, we performed landmark photobleaching with animals expressing laminin::GFP. Regions of the BM bordering the expanding gap and at a distance were not different in fluorescence recovery after photobleaching (Figure S2). Thus, reduced BM deposition does not contribute to gap widening.

To examine if the sliding BM is compressed during gap expansion, we photoconverted alternating 5μm wide stripes of laminin::Dendra adjacent to the expanding BM gap. These stripes were not compressed and shifted in relation to the underlying vulval cells (Figure 4B and 4E; Figure S1). During the time of BM gap expansion, we found that the vulval and uterine tissue increased nearly two fold in size (1.7 and 2.0 fold, respectively), suggesting that the displaced BM was spreading over the growing tissues. Taken together, these results indicate that BM shifting underlies gap expansion during uterine-vulval attachment.

Vulval Expressed INA-1/PAT-3 (Integrin) Restricts BM Gap Expansion

To determine the molecular mechanisms that regulate BM gap formation, we conducted a focused screen and examined 15 strains containing mutant alleles of genes encoding secreted and transmembrane proteins whose RNAi knockdown leads to uterine-vulval attachment defects (WormBase Release WS210; Table S3). We found that animals harbouring a hypomorphic mutation in one of these genes, the integrin α subunit *ina-1(gm39)* [37], had a weakly penetrant BM gap positioning defect, with 13% of observed gaps showing an over-expanded boundary at the mid L4 stage (Figure 5A; Table 1). Integrin receptors are composed of a single α and β subunit and mediate cell-matrix interactions [38]. *C. elegans* possess two integrin receptors, comprised of the α subunits INA-1 (similar to vertebrate laminin-binding integrins) or PAT-2 (similar to vertebrate RGD-binding integrins) bound with the lone β subunit, PAT-3 [32]. As null alleles in all of these genes lead to embryonic or early larval lethality, we utilized vulval- (*unc-62 > rde-1*) and uterine-specific (*fos-1a > rde-1*) RNAi strains to further examine their functions [13,33]. RNAi-targeted depletion of *ina-1*, *pat-2* or *pat-3* in the uterine tissue (*fos-1a > rde-1* strain) did not significantly alter BM gap positioning (Table 1). RNAi targeted knock down of *ina-1* and *pat-3* in the vulval tissue (*unc-62 > rde-1* strain), however, caused an overexpansion defect, similar to *ina-1(gm39)* mutants (Table 1). No defects in BM gap formation were observed after RNAi depletion of *pat-2* in the vulval tissue (Table 1). These results suggest that the INA-1/PAT-3 heterodimer functions in the vulval cells to restrict BM gap opening.

Similar to *Drosophila* and vertebrate cells, we have found that α and β integrin subunits require heterodimerization within the secretory apparatus of the uterine and vulval cells to be transported efficiently to the cell surface [33,39,40]. We thus examined the localization of a full length PAT-3::GFP construct cotransformed with genomic DNA encoding INA-1 or PAT-2 [33]. Cotransformation of *pat-3::GFP* with *ina-1* showed enriched PAT-3::GFP localization at the site of the BM gap boundary position during the mid L4 stage (Figure 5B–D). Mosaic expression studies indicated that the boundary localized INA-1/PAT-3::GFP was derived from the vulval cells, most strongly within the vulD cells (Figure S3).

Consistent with a function here, expression of a dominant negative integrin β subunit PAT-3 construct in the vulD and neighbouring vulC cells driven by the *egl-17* promoter (*egl-17 > HA-βtail*), resulted in a BM gap overexpansion defect (Table 1). Neither *ina-1(gm39)* nor *egl-17 > HA-βtail* animals had alterations in vulval fate specification (Figure S4), supporting a direct role for INA-1/PAT-3 in limiting BM gap expansion. No significant concentrations of PAT-2/PAT-3::GFP integrin were detected in the vulval or uterine cells participating in boundary formation [33]. These studies indicate that vulval localized INA-1/PAT-3 integrin limits BM gap expansion.

Vulval VAB-19 (Kank) Stabilizes BM Gap Position

In a screen for genes expressed during uterine-vulval attachment, we found that a full-length GFP-tagged expression construct for the protein VAB-19, a homolog of the cytoplasmic tumour suppressor protein Kank [26], localized to the site of the BM gap boundary (Figure 5F–H). VAB-19 regulates epithelial cell-matrix attachment structures in the *C. elegans* embryo [25,41], suggesting it might participate in BM gap positioning during uterine-vulval attachment. Null mutations in *vab-19* are embryonic lethal [41]. Thus, we examined BM boundary position in the cold-sensitive mutant *vab-19(e1036)* [41] and found a weakly penetrant defect at a restrictive temperature of 17°C, with 8% of observed BM boundaries over-expanded (Figure 5E; Table 1). Similar to integrin function, vulval- and uterine-specific RNAi mediated knockdown of *vab-19* suggested that *vab-19* functions within the vulval cells (Table 1). Mosaic expression analysis revealed that VAB-19::GFP was also expressed most strongly in the vulD cells at the BM gap boundary, and weakly expressed in the uterine cells (Figure S3). To explore the interaction between integrin and VAB-19 function, we examined *vab-19(e1306)* mutant animals harbouring the vulval-expressed dominant negative integrin *egl-17 > HA-βtail* and found an additive defect in BM gap hyper-expansion (Table 1). These results indicate that integrin and VAB-19 function together, either in the same or parallel pathways, to limit BM gap expansion within the vulval cells.

Vulval and Uterine Cells Function together to Limit BM Gap Expansion

Our data show that VAB-19 and INA-1/PAT-3 function within the vulval cells, in combination with an additional mechanism in the ventral uterine cell descendants to restrict BM gap expansion. To explore the interaction between these mechanisms, we performed ventral uterine cell ablation in *egl-17 > HA-βtail* (vulD expressed dominant negative integrin) animals and found a strong synergistic interaction. Whereas *egl-17 > HA-βtail* and ventral uterine cell ablation each resulted in approximately 20% BM boundaries showing an over-expanded position, the combined perturbations resulted in 80% of BM gap borders being hyper-expanded (Table 1; Figure 6A–C). Similarly, we observed a robust synergistic interaction in *vab-19(e1306)* animals after ventral uterine cell ablation to nearly 60% of BM gap boundaries being over-expanded (Table 1). Importantly, vulval cell division and invagination appeared normal in these animals. Measurements of vulval height and width after reductions of VAB-19 and integrin function revealed no differences compared to wild-type animals (Figure S5), consistent with integrin and VAB-19 functioning directly to limit the sliding of the BM, rather than indirectly through alterations in vulval morphogenesis. Taken together these data support a cooperative function for VAB-19 (Kank) and INA/

PAT-3 (integrin) within the vulval cells and a distinct molecular mechanism operating in the ventral uterine cell descendants that acts to limit BM movement during uterine-vulval attachment.

DISCUSSION

How cells create gaps in BM during normal morphogenetic and pathogenic processes is poorly understood [4,6]. Using uterine-vulval attachment in *C. elegans* as a model for BM remodelling, we show that after the uterine AC breaches the BM, the underlying vulval cells expand and then stabilize the BM gap by promoting BM sliding followed by targeted adhesion at a specific cellular boundary (Summarized in Figure 6D and 6E). This *in vivo* work reveals that a novel mechanism, BM sliding, underlies BM gap enlargement and highlights how collaborative interactions between an invasive cell and tissue invaded can open BM breaches. Notably, cooperative interactions between leukocytes and endothelial cells are thought to promote leukocyte passage through endothelial BM [5,6,42]. Such collaborative interplay may be a common strategy to form BM gaps.

Proteolytic degradation or reduced BM assembly are postulated mechanisms underlying BM gap formation [1]. The fate of the BM lost during these events, however, has not been determined and thus the mechanisms that promote removal remain unclear. By following the fate of the BM through optical highlighting of laminin::Dendra and type IV collagen::Dendra, we show that the BM is not removed by dissolution during uterine-vulval attachment. Further, landmark photobleaching of laminin::GFP revealed no reduction in BM deposition at the expanding gap boundary. Instead, our optical highlighting experiments demonstrate that the BM shifts to expand the gap. As the BM slides at the boundary, the juxtaposed uterine and vulval cells make direct cell-cell connections [27], which likely excludes further BM deposition. During uterine-vulval attachment the uterine and vulval tissue expand nearly two fold in size, supplying the sliding BM enlarged tissue to spread over. Tissue growth might be a prerequisite for BM sliding, providing a surface for the shifted BM to cover. Proteases may also be utilized to facilitate BM sliding, however, our optical highlighting experiments clearly show that these do not dissolve the BM. Notably, proteolysis might be particularly important in initiating the break in the BM, as the *C. elegans* matrix metalloproteinase *zmp-1* is expressed within the AC during invasion and is thought to function during the initial breaching event [21]. The reliance of BM sliding on the number of dividing and invaginating vulval cells suggests that these morphogenetic processes provide the force to move the BM, analogous to migrating fibroblasts shifting collagen fibres in connective tissue matrix [43]. Importantly, the BM sliding model does not preclude an active role for the vulval cells in expanding the gap by migrating into the opening (as opposed to BM sliding over them). However, since vulval morphogenesis was normal in cases with over-expanded borders, we propose BM sliding as the primary mechanism driving BM gap expansion.

Our studies indicate that after the invaginating vulval cells initiate BM sliding, the uterine and vulval cells have independent mechanisms for halting this movement at a specific cellular boundary. Laser ablation of the uterine cells increased the expansion of the BM gap, demonstrating that these cells act to restrict BM movement. Furthermore, the expression

patterns and loss of function phenotypes of the genes encoding the integrin heterodimer INA-1/PAT-3 and the Kank homolog VAB-19, indicate that these proteins act in the vulval vulD cells to limit BM gap expansion (Figure 6E). The INA-1/PAT-3 integrin heterodimer is most similar to vertebrate integrin laminin receptors [37], consistent with a role in cell-BM adhesion. Although the *in vivo* functions of Kank proteins are poorly understood, VAB-19/Kank has also previously been implicated in mediating cell-BM interactions in *C. elegans* [25,41]. VAB-19 is thought

While BMs have been hypothesized to be highly static structures [46–48], there have been few real-time analysis studies of BM dynamics *in vivo*. Recent work examining chick primitive streak formation has shown that the underlying sub-epiblastic extracellular matrix (a matrix similar to BM) moves with the migrating epiblastic cells [49]. Our observations demonstrating that the BM is shifted during gap expansion in uterine-vulval development in *C. elegans* provides further evidence that BM itself can have plastic properties. Similar to uterine-vulval development, the formation of BM gaps during vertebrate gastrulation, *Drosophila* disc eversion, and in metastatic tumours [7,9,50] is associated with dividing and moving cells, where similar conditions to shift BM likely occur. Thus, BM sliding may be a common strategy to widen BM gaps with important implications in the design of therapies to modulate this behaviour.

METHODS

Strains and Culture Conditions

Culturing and handling of *C. elegans* was done as previously described [51]. Wild-type animals were strain N2. In the text and figures, we designated linkage to a promoter with a (>) symbol and use a (::) symbol for linkages that fuse open reading frames. The following alleles and transgenes were used in this study: *qyEx36[pat-3::GFP;genomic ina-1], qyEx76[vab-19::GFP], qyEx43[pat-3::GFP; genomic pat-2], qyIs103[fos-1a > rde-1], qyIs110[egl-17 > HA-βtail], qyIs111[egl-17 > HA-βtail], qyIs138[unc-62 > rde-1], qyIs139[unc-62 > rde-1], qyIs127[laminin::mCherry], qyIs161[emb-9::Dendra], qyIs87[vab-19::GFP], qyIs89[vab-19::GFP], qyIs108[laminin::Dendra], qyIs109[laminin::Dendra], qyIs43[pat-3::GFP;genomic ina-1]*; **LGI**, *ayIs4[egl-17 >GFP], lrp-1(ku156), gld-1(q266), inx-13(ok236), clec(tm1291), dpy-5(e61);* **LGII**, *vab-19(e1036), rrf-3(pk1426), qyIs23[cdh-3 > mCherry::PLCδ^{PH}], clr-1(e1745);* **LGIII**, *unc-119(ed4), ina-1(gm39), ten-1(ok641);* **LGIV**, *lin-3(n1059), lin-3(n378), let-653(s1733), tag-144(ok750), qyIs42[pat-3::GFP;genomic ina-1], qyIs15 [zmp-1 > HA-βtail], qyIs10[laminin::GFP];* **LGV**, *mig-6(ev700), rde-1(ne219), qyIs44[emb-9::mCherry], wsp-1(gm324);* **LGX**, *chtl-1(ok1695), him-4(rh319), osm-11(n1604), qyIs24[cdh-3 > mCherry::PLCδ^{PH}], qyIs7[laminin::GFP], qyIs10[laminin::GFP], qyIs46[emb-9::mCherry]*. See Supplementary Tables 4 and 5 for all new transgenic strains and primer sequences for generation of new PCR fusion constructs.

Microscopy, Image Acquisition, Processing and Analysis

Images were acquired using a Yokogawa spinning disk confocal mounted on a Zeiss AxioImager microscope with a 100× Plan-APOCHROMAT objective controlled by iVision software (Biovision Technologies, Exton, PA) or using a Zeiss AxioImager microscope with

a 100× Plan-APOCHROMAT objective equipped with a Zeiss AxioCam MRm CCD camera controlled by Axiovision software (Zeiss Microimaging, Inc., Thornwood, NJ). Acquired images were processed using Photoshop CS3 Extended (Adobe Systems, Inc., San Jose, CA). Three-dimensional reconstructions were built from confocal z-stacks, analyzed, and exported as (.mov) files using IMARIS 6.0 (Bitplane, Inc., Saint Paul, MN). Spectral representations of the fluorescent intensities of VAB-19::GFP and PAT-3::GFP expression (two independent lines each) were constructed using Image J 1.40 g software.

Uterine-vulval Tissue Separation

To visualize the relationship between the gonadal and ventral epidermal BMs (which are normally tightly juxtaposed and cannot be resolved by light microscopy) we incubated worms for one hour in M9, under a cover slip, on a 5% agar pads containing 0.01M NaN_3. Under these conditions, the uterine and vulval tissues can separate from one another allowing their respective BMs to be individually visualized.

Mosaic Analysis of VAB-19::GFP and PAT-3::GFP Expression

Because the uterine and vulval tissues are tightly juxtaposed, a mosaic expression analysis was conducted to determine the origin of the VAB-19 and INA-1/PAT-3 that localized at the BM gap boundary. *qyEx36[pat-3::GFP;genomic ina-1]* and *qyEx76[vab-19::GFP]* lines were examined for somatic loss of the transgene in either the uterine or vulval lineage (determined by absence of fluorescence in the tissue), but the complementary presence in the vulval or uterine lineage, respectively.

Cell Ablations

Laser-directed cell ablations of the AC, VU, DU and VPC cells were performed on 5% agar pads as previously described [8]. Ablated animals were recovered from the agar pad, allowed to develop at 20°C, and then examined for AC invasion and boundary position defects at indicated times.

RNA Interference

Double-strand RNA (dsRNA) used in this study was delivered by feeding to *wsp-1(gm324), qyIs23[cdh-3 > mCherry::PLCδ^{PH}], qyIs10[laminin::GFP], rrf-3(pk1426)*, uterine- (*fos-1a > rde-1*) and VPC-specific (*unc-62 > rde-1*) RNAi sensitive strains. VPC- and uterine-specific RNAi was conducted by expression RDE-1 under the control of the vulval specific *unc-62* promoter [13] and the uterine specific *fos-1a* promoter as described [33]. Tissue specificity of both was confirmed with RNAi targeting genes that have known specific functions in the uterine (*pat-3, fos-1a*) and vulval (*lin-39*) tissues. All RNAi vectors were from the Vidal or Ahringer libraries [52,53] and sequenced to verify correct insert.

Quantifying the Breach in the BM

The diameter of the breach in BM was measured at five developmental stages: P6.p four-, late four-, six-, early eight- and eight-cell stages. The position of the BM breach was scored either by visualization of the phase-dense line under DIC optics or by localization of laminin::GFP. In all cases an unpaired Student's *t*-test was used to determine the statistical

significance of observed differences between stages. The anterior and posterior boundaries of the breach were scored independently at the early L4 and mid L4 larval stages (see Table 1).

Optical Highlighting (Photoconversion) of Basement Membrane Components

Dendra DNA sequence [36] was engineered to contain *C. elegans* codon usage [54] and three synthetic introns (sequence is available upon request). Dendra fusion constructs were made by inserting the *C. elegans* modified Dendra into the mluI site of pGK39 (*laminin::GFP*) and the Msc1 and BsrG1 sites of pJK750 (*type IV collagen::mCherry*). Constructs were injected and integrated strains made as described previously [21]. Transgenic worms were photoconverted using a Zeiss LSM 510 confocal (Zeiss Microimaging, Inc., Thornwood, NJ), equipped with a 63× objective, scanning regions of interest with a 405 nm laser at 1 mW power for 30s. After photoconversion, images were captured using a spinning disc confocal or a Zeiss AxioImager. Animals were recovered from the agar pad, allowed to develop at 20°C for the specified amount of time, and then reimaged. Identical settings were used to acquire images at all time points. The sum fluorescence intensity of photoconverted Dendra was quantified using Image J 1.40 g software and a seven-pixel-wide linescan. For more details on photoconversion of BM methods used in this study see Nature Protocols.

Volumetric Measurements of Uterine and Vulval Tissues

Three-dimensional isosurface renderings were generated from confocal z-stacks of vulval- or uterine-specific GFP expression (*unc-62>GFP* and *fos-1>GFP* strains, respectively), using Imaris 7.1.1 (Bitplane, Inc. Saint Paul, MN). A fluorescence intensity threshold was set so isosurfaces were built in place of the uterine or vulval tissue. The volume of isosurfaces was used to estimate the volume of the respective tissue at the 4- and 8-cell stage ($n \geq 8$ for each).

Supplementary Material

Refer to Web version on PubMed Central for supplementary material.

ACKNOWLEDGEMENTS

We are grateful to A. Chisholm for the *vab-19::GFP* vector; J. Culotti for the *mig-6(ev700)* strain; J. Schwarzbauer for the *pat-3* HA-βtail vector; Shohei Mitani for the deletion mutant (*tm1291*), S. Johnson of the Duke University LMCF for imaging advice, strains provided by the *Caenorhabditis* Genetic Center, and A. Schindler, D. Matus and L. Lilley for helpful comments on the manuscript. This work was supported by a Basil O'Connor Scholars Research Award, The Pew Scholars Program in the Biomedical Sciences and NIH Grant GM079320 and GM079320-03S1 to D.R.S., HD027211 to J.M.K. and a JSPS Postdoctoral Fellow for Research Abroad Award to S.I.

REFERENCES

1. Rowe RG, Weiss SJ. Navigating ECM barriers at the invasive front: the cancer cell-stroma interface. Annu Rev Cell Dev Biol. 2009; 25:567–595. [PubMed: 19575644]
2. Sherwood DR. Cell invasion through basement membranes: an anchor of understanding. Trends Cell Biol. 2006; 16:250–256. [PubMed: 16580836]
3. Kalluri R. Basement membranes: structure, assembly and role in tumour angiogenesis. Nat Rev Cancer. 2003; 3:422–433. [PubMed: 12778132]

4. Even-Ram S, Yamada KM. Cell migration in 3D matrix. Curr Opin Cell Biol. 2005; 17:524–532. [PubMed: 16112853]
5. Rowe RG, Weiss SJ. Breaching the basement membrane: who, when and how? Trends Cell Biol. 2008; 18:560–574. [PubMed: 18848450]
6. Nourshargh S, Hordijk PL, Sixt M. Breaching multiple barriers: leukocyte motility through venular walls and the interstitium. Nat Rev Mol Cell Biol. 2010; 11:366–378. [PubMed: 20414258]
7. Nakaya Y, Sukowati EW, Wu Y, Sheng G. RhoA and microtubule dynamics control cell-basement membrane interaction in EMT during gastrulation. Nat Cell Biol. 2008; 10:765–775. [PubMed: 18552836]
8. Sherwood DR, Sternberg PW. Anchor cell invasion into the vulval epithelium in C. elegans. Dev Cell. 2003; 5:21–31. [PubMed: 12852849]
9. Srivastava A, Pastor-Pareja JC, Igaki T, Pagliarini R, Xu T. Basement membrane remodeling is essential for Drosophila disc eversion and tumor invasion. Proc Natl Acad Sci U S A. 2007; 104:2721–2726. [PubMed: 17301221]
10. Barsky SH, Siegal GP, Jannotta F, Liotta LA. Loss of basement membrane components by invasive tumors but not by their benign counterparts. Lab Invest. 1983; 49:140–147. [PubMed: 6348406]
11. Flug M, Kopf-Maier P. The basement membrane and its involvement in carcinoma cell invasion. Acta Anat (Basel). 1995; 152:69–84. [PubMed: 7660759]
12. Frei JV. The fine structure of the basement membrane in epidermal tumors. J Cell Biol. 1962; 15:335–342. [PubMed: 13959516]
13. Matus DQ, et al. In vivo identification of regulators of cell invasion across basement membranes. Sci Signal. 2010; 3:ra35. [PubMed: 20442418]
14. Spaderna S. A transient, EMT-linked loss of basement membranes indicates metastasis and poor survival in colorectal cancer. Gastroenterology. 2006; 131:830–840. [PubMed: 16952552]
15. Cavallo-Medved D, et al. Live-cell imaging demonstrates extracellular matrix degradation in association with active cathepsin B in caveolae of endothelial cells during tube formation. Exp Cell Res. 2009; 315:1234–1246. [PubMed: 19331819]
16. Garbisa S, Kniska K, Tryggvason K, Foltz C, Liotta LA. Quantitation of basement membrane collagen degradation by living tumor cells in vitro. Cancer Lett. 1980; 9:359–366. [PubMed: 7397689]
17. Hotary K, Li XY, Allen E, Stevens SL, Weiss SJ. A cancer cell metalloprotease triad regulates the basement membrane transmigration program. Genes Dev. 2006; 20:2673–2686. [PubMed: 16983145]
18. Overall CM, Kleifeld O. Tumour microenvironment - opinion: validating matrix metalloproteinases as drug targets and anti-targets for cancer therapy. Nat Rev Cancer. 2006; 6:227–239. [PubMed: 16498445]
19. Page-McCaw A, Ewald AJ, Werb Z. Matrix metalloproteinases and the regulation of tissue remodelling. Nat Rev Mol Cell Biol. 2007; 8:221–233. [PubMed: 17318226]
20. Sameni M, Dosescu J, Yamada KM, Sloane BF, Cavallo-Medved D. Functional live-cell imaging demonstrates that beta1-integrin promotes type IV collagen degradation by breast and prostate cancer cells. Mol Imaging. 2008; 7:199–213. [PubMed: 19123990]
21. Sherwood DR, Butler JA, Kramer JM, Sternberg PW. FOS-1 promotes basement-membrane removal during anchor-cell invasion in C. elegans. Cell. 2005; 121:951–962. [PubMed: 15960981]
22. Xu J, et al. Proteolytic exposure of a cryptic site within collagen type IV is required for angiogenesis and tumor growth in vivo. J Cell Biol. 2001; 154:1069–1079. [PubMed: 11535623]
23. Liotta LA, Rao NC, Barsky SH, Bryant G. The laminin receptor and basement membrane dissolution: role in tumour metastasis. Ciba Found Symp. 1984; 108:146–162. [PubMed: 6240391]
24. Newman AP, Sternberg PW. Coordinated morphogenesis of epithelia during development of the Caenorhabditis elegans uterine-vulval connection. Proc Natl Acad Sci U S A. 1996; 93:9329–9333. [PubMed: 8790329]

25. Ding M, et al. The cell signaling adaptor protein EPS-8 is essential for C. elegans epidermal elongation and interacts with the ankyrin repeat protein VAB-19. PLoS One. 2008; 3:e3346. [PubMed: 18833327]
26. Kakinuma N, Zhu Y, Wang Y, Roy BC, Kiyama R. Kank proteins: structure, functions and diseases. Cell Mol Life Sci. 2009; 66:2651–2659. [PubMed: 19554261]
27. Newman AP, White JG, Sternberg PW. Morphogenesis of the C. elegans hermaphrodite uterus. Development. 1996; 122:3617–3626. [PubMed: 8951077]
28. Lints R, Hall DH. Reproductive system, egglaying apparatus. WormAtlas. 2010 doi:10.3908/wormatlas.3901.3924.
29. Kao G, Huang CC, Hedgecock EM, Hall DH, Wadsworth WG. The role of the laminin beta subunit in laminin heterotrimer assembly and basement membrane function and development in C. elegans. Dev Biol. 2006; 290:211–219. [PubMed: 16376872]
30. Ziel JW, Hagedorn EJ, Audhya A, Sherwood DR. UNC-6 (netrin) orients the invasive membrane of the anchor cell in C. elegans. Nat Cell Biol. 2009; 11:183–189. [PubMed: 19098902]
31. Fitzgerald MC, Schwarzbauer JE. Importance of the basement membrane protein SPARC for viability and fertility in Caenorhabditis elegans. Curr Biol. 1998; 8:1285–1288. [PubMed: 9822581]
32. Kramer JM. Basement membranes. WormBook. 2005:1–15. [PubMed: 18050423]
33. Hagedorn EJ, et al. Integrin acts upstream of netrin signaling to regulate formation of the anchor cell's invasive membrane in C. elegans. Dev Cell. 2009; 17:187–198. [PubMed: 19686680]
34. Kimble J, Hirsh D. The postembryonic cell lineages of the hermaphrodite and male gonads in Caenorhabditis elegans. Dev Biol. 1979; 70:396–417. [PubMed: 478167]
35. Liu J, Tzou P, Hill RJ, Sternberg PW. Structural requirements for the tissue-specific and tissue-general functions of the Caenorhabditis elegans epidermal growth factor LIN-3. Genetics. 1999; 153:1257–1269. [PubMed: 10545457]
36. Gurskaya NG, et al. Engineering of a monomeric green-to-red photoactivatable fluorescent protein induced by blue light. Nat Biotechnol. 2006; 24:461–465. [PubMed: 16550175]
37. Baum PD, Garriga G. Neuronal migrations and axon fasciculation are disrupted in ina-1 integrin mutants. Neuron. 1997; 19:51–62. [PubMed: 9247263]
38. Yurchenco PD, Amenta PS, Patton BL. Basement membrane assembly, stability and activities observed through a developmental lens. Matrix Biol. 2004; 22:521–538. [PubMed: 14996432]
39. Leptin M, Bogaert T, Lehmann R, Wilcox M. The function of PS integrins during Drosophila embryogenesis. Cell. 1989; 56:401–408. [PubMed: 2492451]
40. Marlin SD, Morton CC, Anderson DC, Springer TA. LFA-1 immunodeficiency disease. Definition of the genetic defect and chromosomal mapping of alpha and beta subunits of the lymphocyte function-associated antigen 1 (LFA-1) by complementation in hybrid cells. J Exp Med. 1986; 164:855–867. [PubMed: 3528378]
41. Ding M, Goncharov A, Jin Y, Chisholm AD. C. elegans ankyrin repeat protein VAB-19 is a component of epidermal attachment structures and is essential for epidermal morphogenesis. Development. 2003; 130:5791–5801. [PubMed: 14534136]
42. Madsen CD, Sahai E. Cancer dissemination--lessons from leukocytes. Dev Cell. 2010; 19:13–26. [PubMed: 20643347]
43. Wolf K, et al. Multi-step pericellular proteolysis controls the transition from individual to collective cancer cell invasion. Nat Cell Biol. 2007; 9:893–904. [PubMed: 17618273]
44. Altun ZF, Hall DH. Muscle system, somatic muscle. WormAtlas. 2010
45. Cox EA, Tuskey C, Hardin J. Cell adhesion receptors in C. elegans. J Cell Sci. 2004; 117:1867–1870. [PubMed: 15090591]
46. Leardkamolkarn V, Abrahamson DR. Binding of intravenously injected antibodies against laminin to developing and mature endocrine glands. Cell Tissue Res. 1988; 251:171–181. [PubMed: 3342435]
47. Price RG, Spiro RG. Studies on the metabolism of the renal glomerular basement membrane. Turnover measurements in the rat with the use of radiolabeled amino acids. J Biol Chem. 1977; 252:8597–8602. [PubMed: 925014]

48. Trier JS, Allan CH, Abrahamson DR, Hagen SJ. Epithelial basement membrane of mouse jejunum. Evidence for laminin turnover along the entire crypt-villus axis. J Clin Invest. 1990; 86:87–95. [PubMed: 2195064]
49. Zamir EA, Rongish BJ, Little CD. The ECM moves during primitive streak formation--computation of ECM versus cellular motion. PLoS Biol. 2008; 6:e247. [PubMed: 18922043]
50. Hanahan D, Weinberg RA. The hallmarks of cancer. Cell. 2000; 100:57–70. [PubMed: 10647931]
51. Brenner S. The genetics of Caenorhabditis elegans. Genetics. 1974; 77:71–94. [PubMed: 4366476]
52. Fraser AG, et al. Functional genomic analysis of C. elegans chromosome I by systematic RNA interference. Nature. 2000; 408:325–330. [PubMed: 11099033]
53. Rual JF, et al. Toward improving Caenorhabditis elegans phenome mapping with an ORFeome-based RNAi library. Genome Res. 2004; 14:2162–2168. [PubMed: 15489339]
54. Green RA, et al. Expression and imaging of fluorescent proteins in the C. elegans gonad and early embryo. Methods Cell Biol. 2008; 85:179–218. [PubMed: 18155464]

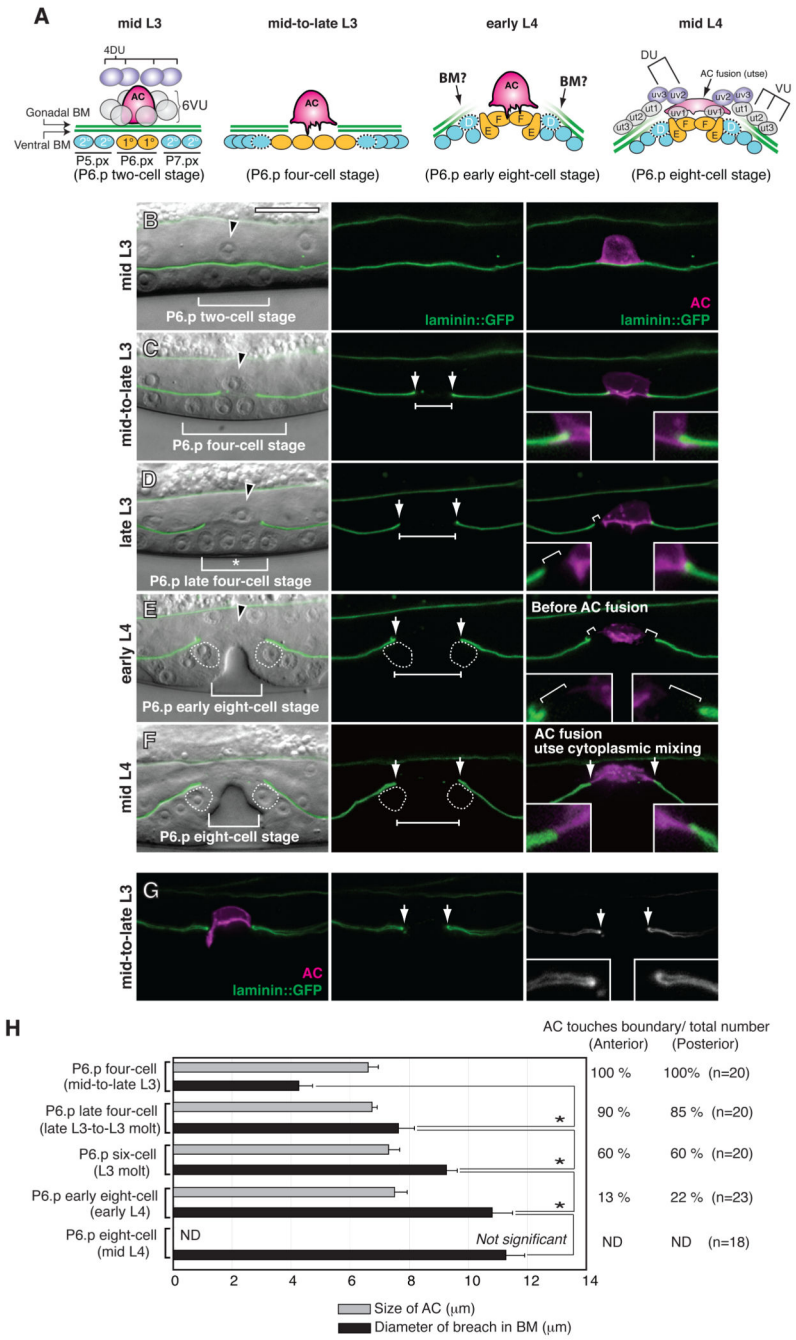

Figure 1. The Gap in the BM Expands during Uterine-vulval Attachment

(A) Diagram depicting uterine-vulval attachment. At the late L3 larval stage, all of the VPCs (vulval precursors cells below the BM) divide except for the 2° fated vulD cells (dotted white line) while the AC moves between the central 1° fated VPCs (vulF cells) at the apex of invaginating vulva. The fate of the BM is unknown during the later phases of uterine-vulval attachment. (VU, ventral uterine cell; DU, dorsal uterine cell). (B–F) Anterior is left and ventral is down, black arrowheads indicate AC and scale bar represents 10μm in this and all subsequent figures. Differential interference contrast (DIC) images overlaid with BM

fluorescence (left) or fluorescent images show the uterine-vulval region of wild-type hermaphrodites. The AC and BM are visualized with *cdh-3* > mCherry::PLCδ^{PH} (magenta) and laminin::GFP (green), respectively. (B) At the mid L3, intact BM separates the uterine and vulval tissues and the AC sits directly over the P6.p 1° VPC daughters (brackets). (C) By the mid-to-late L3 stage, AC invasion has generated a BM gap (white arrows, boundary; white bar, diameter in this and all subsequent figures). At this time, the AC is in contact with the BM (right panel, insets). (D) During the late L3 stage, the central 1° VPCs invaginate (asterisk) and the BM gap expands beyond the AC (inverted bracket). (E) By the early L4 stage, the 1° VPCs have divided again and are out of the plane of focus. The expanding gap stabilizes over the vulD cells (dotted white line in this and all subsequent figures) abutting the multinucleate utse cell (insets) by the mid L4 stage (F). (G) Merged fluorescence is left, BM fluorescence, centre and grayscale, right. After AC invasion, separation of the uterine and vulval tissues revealed that the gonadal and ventral epidermal BMs fused bordering the site of invasion (white arrows, insets). (H) Bar graph reports the diameter of AC and BM gap at each stage. The P6.p six-cell stage is when the outer P6.p granddaughters have divided. Asterisks denote statistically significant difference ($p < 0.05$; Student's *t*-test). Error bars report the standard error of the mean.

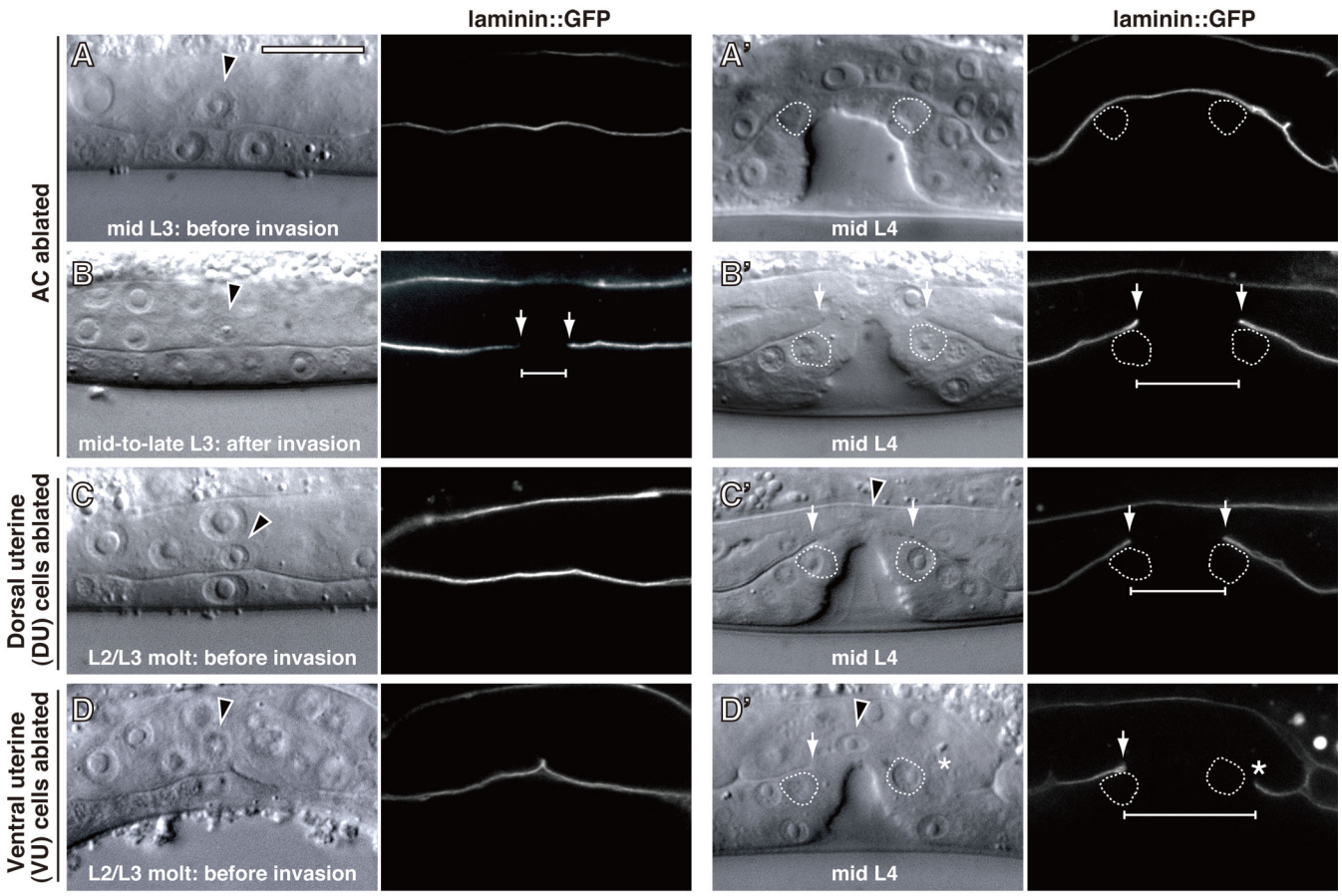

Figure 2. The Role of the Uterine Cells during BM Gap Formation

(A–D) DIC image (left) and corresponding confocal section of BM viewed with laminin::GFP (green, right) show animals prior to laser-directed cell ablation. (A'–D') Similar images show corresponding animals after laser ablation at the mid L4 stage. (A) When the AC was killed by laser ablation just prior to invasion (P6.p two-cell stage), the BM separating the uterine and vulval tissues remained intact later at the mid L4 stage (A'). (B) When the AC was ablated just after invasion (P6.p four-cell stage), BM gap expansion was normal (B'). (C) Laser ablation of the dorsal uterine cells that sit above the AC at L2/L3 molt (P6.p one-cell stage) had no effect on uterine-vulval attachment or BM gap formation (C'). (D) Ablation of the ventral uterine cells at L2/L3 molt resulted in an overexpansion of the BM gap past the vulD cells in 20% of the BM boundaries examined (D', asterisk indicates overexpansion at the posterior boundary).

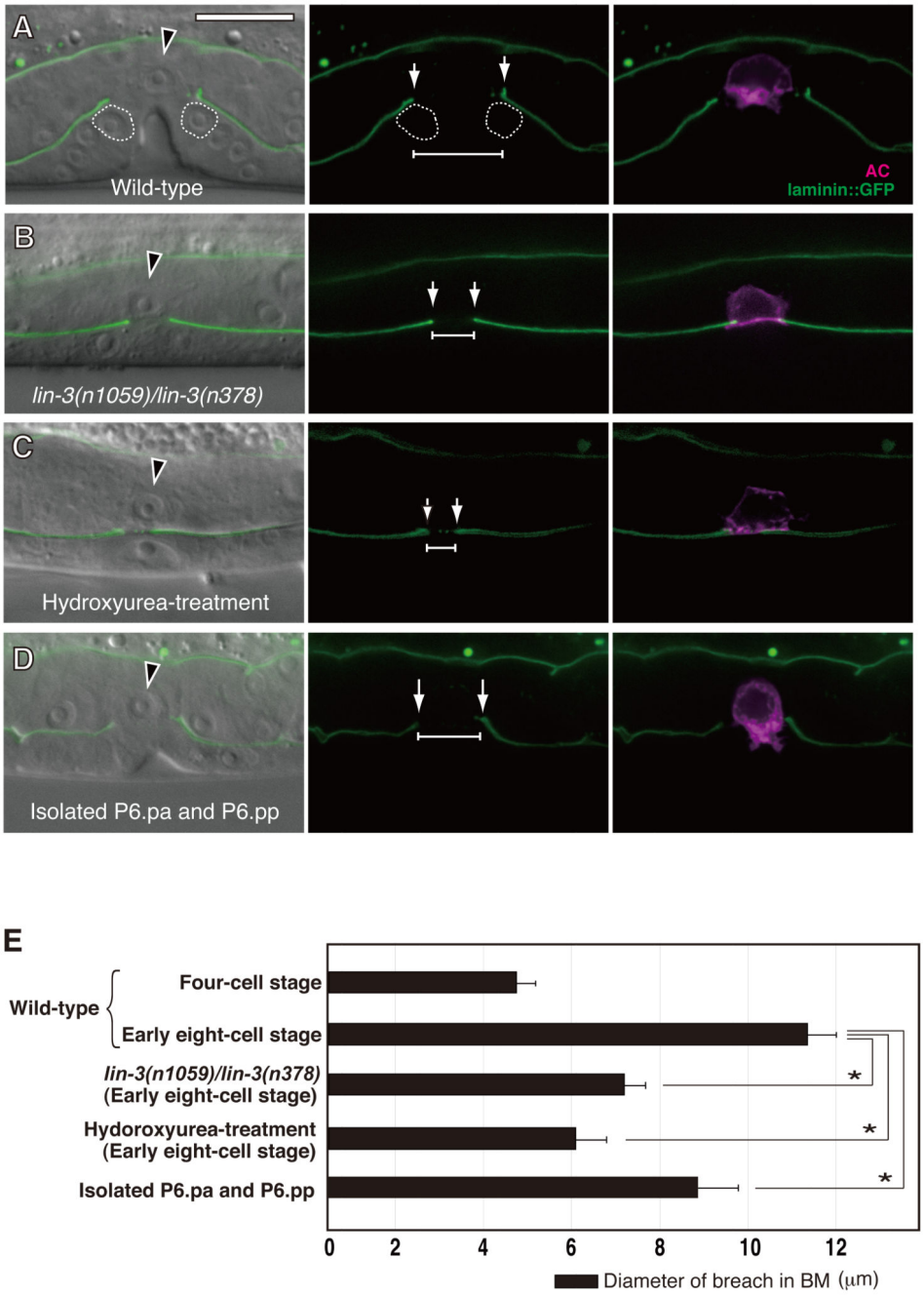

Figure 3. The VPCs Expand the Breach in the BM

(A–D) DIC image overlaid with confocal section of BM visualized with laminin::GFP (green, left), BM fluorescence alone (middle), and AC (expressing *cdh-3* > mCherry::PLCδ^{PH}, magenta) with BM (right) in early L4 stage animals. (A) By the early L4 stage in wild-type animals (P6.p early eight-cell stage), the BM gap expanded and stabilized over the vulD cells. (B) When the AC invaded in a vulvaless animals (*lin-3(n1059)/ lin-3(n378)*), the gap that formed in the BM never expanded beyond the AC. (C) Similarly, when vulval cell division was blocked by hydroxyurea treatment, the BM gap never

expanded beyond the AC. (D) Laser-directed killing of all VPCs, except P6.pa and P6.pp, which give rise to the vulF cells (see Figure 1A), resulted in a reduction in BM gap enlargement. (E) Bar graph reports the average diameter of the breach generated in the BM in wild-type, vulvaless, hydroxyurea-treatment animals and isolated P6.pa and P6.pp cells (n = 10 animals examined for each treatment). The asterisks denote a statistically significant difference ($p < 0.05$; Students *t*-test). Error bars report the standard error of the mean.

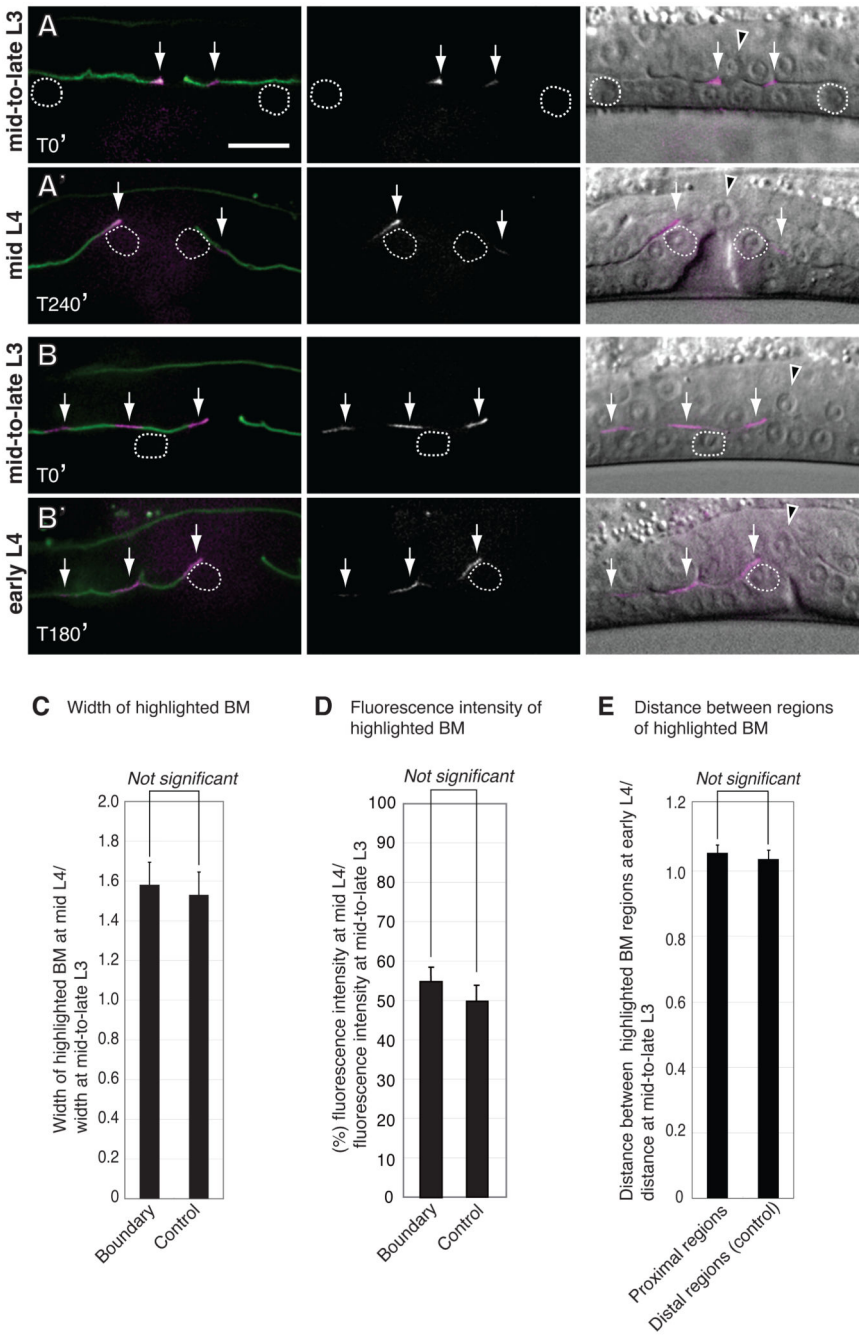

Figure 4. BM Sliding underlies BM GAP Enlargement

(A–B) Fluorescence overlays show laminin::Dendra after localized exposure to 405nm light (white arrows point to optically highlighted (photoconverted) regions of laminin::Dendra, shown in magenta; left). Corresponding images show only photoconverted laminin::Dendra (middle, grayscale), and laminin::Dendra overlaid on DIC (right, magenta). Time-points are shown in minutes, T0' is the time at which the laminin::Dendra was first photoconverted. (A) Two 5μm wide regions of laminin::Dendra were photoconverted; one at the anterior boundary of the gap and a second region several microns posterior to the gap (control). (A')

The same animal shown in A, 240 minutes later. The photoconverted region of laminin::Dendra was not lost and shifted from a location over the vulF precursor cell to occupy a position over the vulD cell (n = 33/33 animals). (B) Three regions of laminin::Dendra were photoconverted; one at the edge of the BM gap, and two at distances anterior to the gap. (B') The animal shown in B, 180 minutes later. (C) Quantification of the width of the regions at the mid L4 stage compared to the width of the regions at the mid-to-late L3 stage (detailed method is shown in Figure S1). (D) Bar graph reports average ratio of fluorescence intensity at mid L4 compared to the fluorescence intensity at time of photoconversion during the mid-to-late L3. (E) Quantification of the distance between the regions at the early L4 stage to the distance between the regions at the mid-to-late L3 (detailed method is shown in Figure S1; n =10 animals for each experiment). No statistical differences between experimental and control highlighted regions were observed ($P > 0.05$, Student's *t*-test). Error bars report the standard error of the mean.

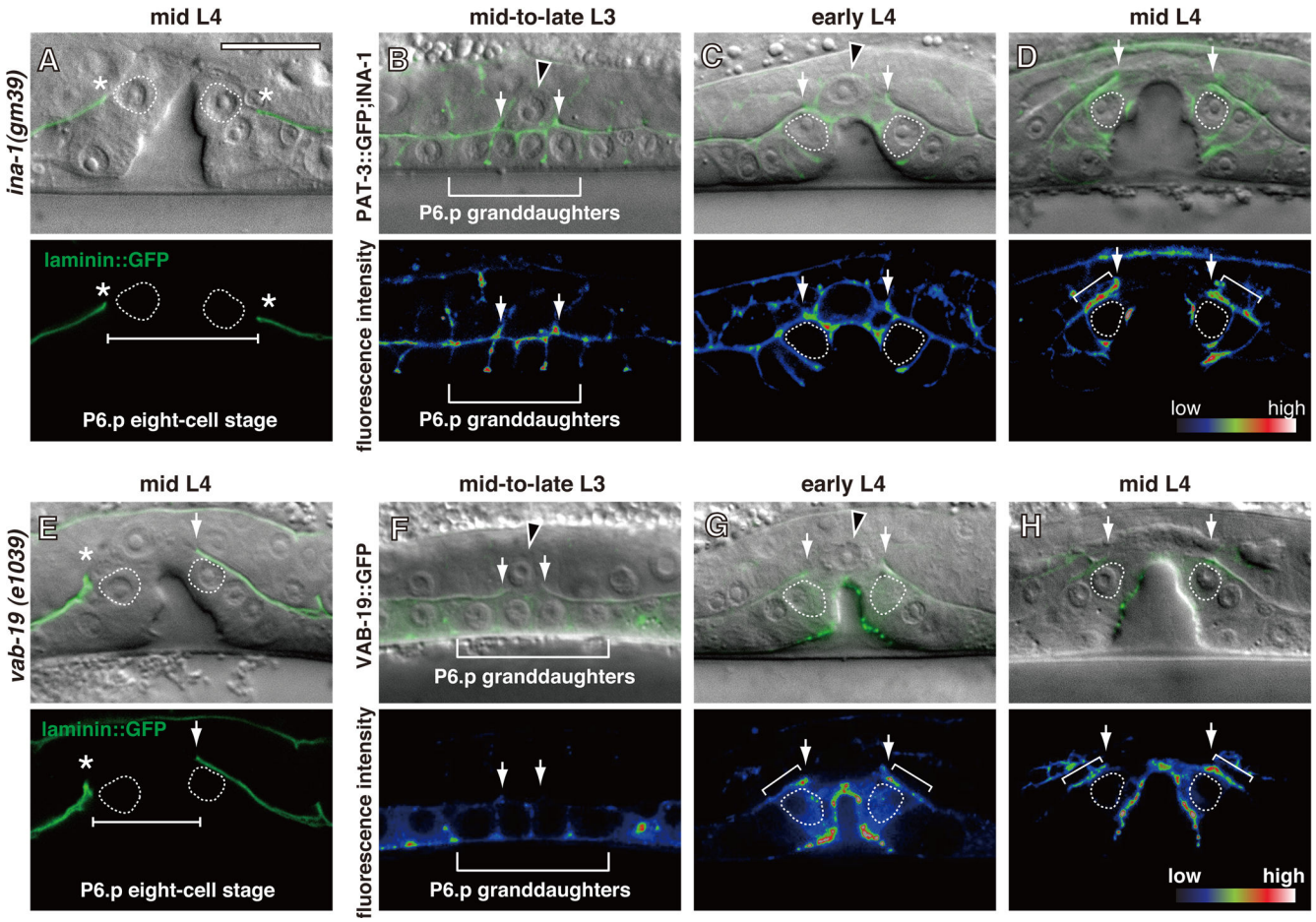

Figure 5. INA-1/PAT-3 (Integrin) and VAB-19 (Kank) Stabilize the BM Gap Boundary

(A and E) DIC images overlaid with BM fluorescence (visualized with laminin::GFP, upper) and BM fluorescent image alone (lower). (B–D and F–H) DIC image overlaid with PAT-3::GFP and VAB-19::GFP fluorescence (green), respectively (upper) and corresponding spectral representation of the fluorescence intensity (lower). (A) Images show an *ina-1(gm39)* mutant where the gap in the BM has expanded beyond the vulD cells (asterisks). (B–D) PAT-3::GFP was expressed throughout the uterine and vulval tissues at the mid-to-late L3 stage and became enriched (inverted brackets) at the boundary of the BM gap (arrows) by the mid L4 stage (n = 51/60 animals examined). (E) Images show a *vab-19(e1039)* mutant where the gap in the BM has over-expanded on the anterior side (asterisk). (F–H) VAB-19::GFP localized to sites of cell-cell contact within the uterine and vulval tissues at mid-to-late L3 (F) and became enriched (inverted brackets) at the boundary of the gap in BM at the early and mid L4 larval stages (n = 57/60 animals; G and H).

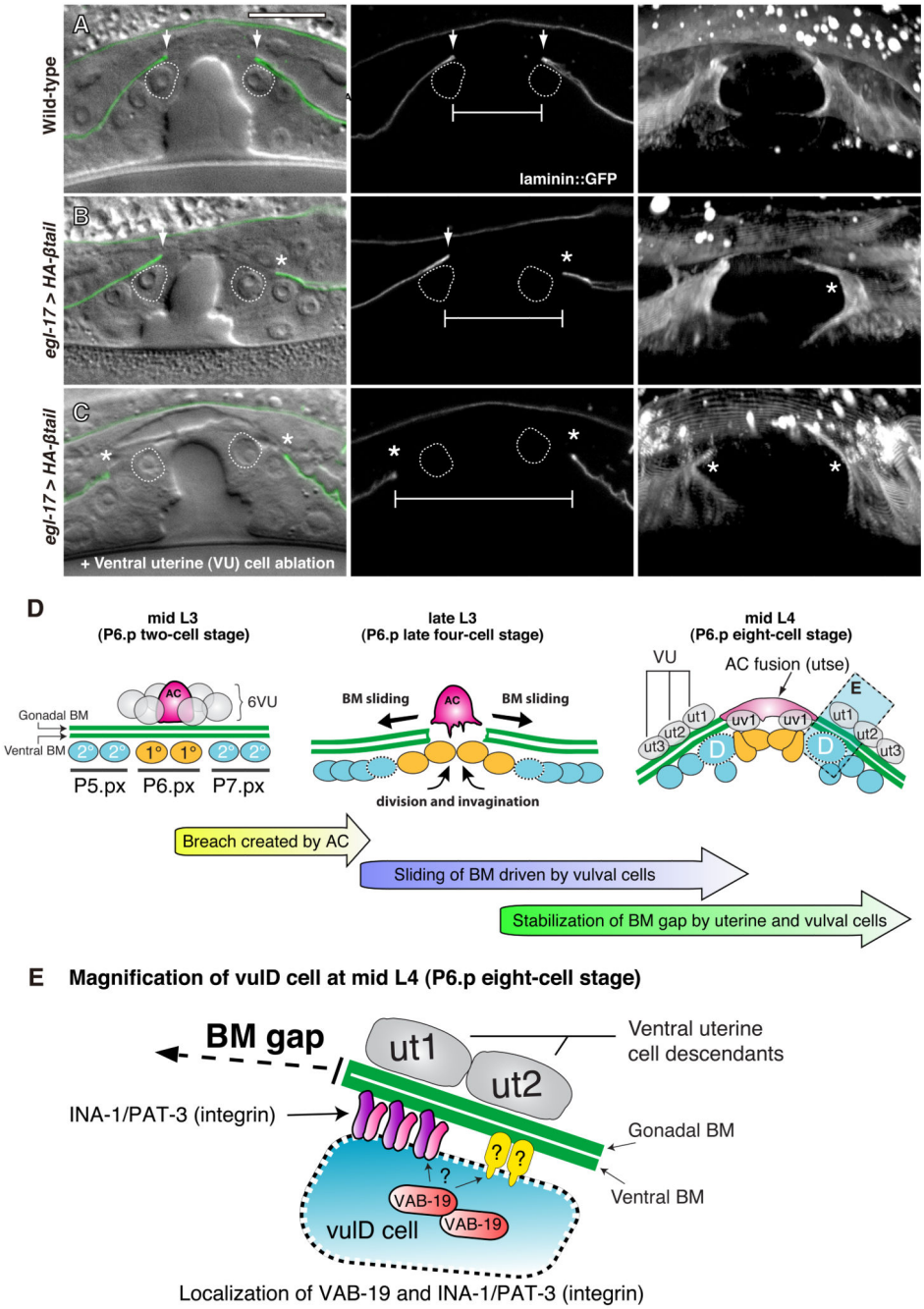

Figure 6. The Uterine and Vulval Cells Act Together to Limit BM Gap Expansion

(A–C) DIC overlaid with BM fluorescence (visualized with laminin::GFP, green, left), grayscale of BM fluorescence (middle), and corresponding 3D reconstruction of an entire confocal z-stack of the BM fluorescence (right, rotated 45° forward). (A) In wild-type animals, the boundary of the gap in the BM stabilized over the vulD cells. (B) Expression of a dominant negative PAT-3 β-integrin construct (HA-βtail) in the vulD cells (*zmp-1 > HA-βtail*) caused overexpansion of the final position of the posterior BM gap boundary (asterisk) at the mid L4 larval stage, also seen in the 3D reconstruction (right). (C) Ventral uterine cell

ablation in animals expressing the HA-βtail construct within the vulD cells resulted in a stronger overexpansion defect than either perturbation alone. (D) Schematic diagram depicts three stages of BM gap formation during uterine-vulval attachment. At the mid L3 larval stage the uterine and vulval tissues are separated by the ventral and gonadal BMs. The AC initiates the breach in the BM at the mid-to-late L3 larval stage. Following AC invasion, the dividing and invaginating vulval cells promote BM sliding to expand the BM gap (arrows). At the early-to-mid L4 stage BM sliding is halted over the vulD cells by INA-1/PAT-3 (integrin) and VAB-19 (homolog of human tumour suppressor Kank) activity within the vulD cells, and a distinct adhesion mechanism that functions within the ventral uterine cell descendants. (E) Enlarged view of attachment site shows INA-1/PAT-3 and VAB-19 as well as the ventral uterine descendants ut1 and ut2 cells stabilizing the boundary of the gap that forms in the BM. VAB-19 may function with integrin or an alternative protein that binds to BM.

Table 1

BM Gap Position During Uterine-vulval Attachment

Genotype/Treatment	BM Gap Position[a]			
	P6.p early 8-cell stage (early L4 stage)		P6.p 8-cell stage (mid L4 stage)	
	% Expanded Gap Boundary [a]	n =	% Expanded Gap Boundary [a]	n =
Wild-type (N2)	0.0	100	3.0	100
Cell Ablation				
AC ablation at P6.p two-cell stage; wild-type (N2)	ND	16	BM intact	16
AC ablation at P6.p early four-cell stage; wild-type (N2)	ND		0	60
3 VU cells ablation; wild-type (N2)	ND		19.4	62
2 DU cells ablation; wild-type (N2)	ND		1.9	54
Integrin				
ina-1(gm39)	6.0	100	13.0	100
qyIs110[egl-17 >HA-βtail] [b]	5.0	60	22.2	90
ina-1 (RNAi); qyIs138[unc-62 >rde-1]; rde-1(ne219); rrf-3(pk1426) [c]	8.8	80	19	100
pat-2 (RNAi); qyIs138[unc-62 >rde-1]; rde-1(ne219); rrf-3(pk1426) [c]	1	100	4	100
pat-3 (RNAi); qyIs138[unc-62 >rde-1]; rde-1(ne219); rrf-3(pk1426) [c]	5.8	70	17.4	80
ina-1 (RNAi); qyIs103[fos-1a >rde-1]; rde-1(ne219); rrf-3(pk1426) [c]	1.7	60	5	80
pat-2 (RNAi); qyIs103[fos-1a >rde-1]; rde-1(ne219); rrf-3(pk1426) [c]	0	60	3.8	80
pat-3 (RNAi); qyIs103[fos-1a >rde-1]; rde-1(ne219); rrf-3(pk1426) [c]	1.7	60	4.5	90
vab-19				
vab-19(e1036) [d]	2.5	80	7.8	90
vab-19 (RNAi); qyIs138[unc-62>rde-1]; rde-1(ne219); rrf-3(pk1426) [c]	5.6	90	12.5	90
vab-19 (RNAi); qyIs103[fos-1a>rde-1];rde-1(ne219); rrf-3(pk1426) [c]	0	60	3.3	90
Pathway Interations				
vab-19(e1036); qyIs110[egl-17 >HA-βtail] [d]	6.3	80	31.3	80
3 VU cells ablation; *qyIs110[egl-17 >HA-βtail]*	ND		79.5	64
3 VU cells ablation; *vab-19(e1036)* [d]	ND		56.7	60

[a] Gap expansion was scored by position of anterior and posterior boundaries in relation to the vulD cell under DIC optics. The BM boundary in wild-type animals is located over the vulD cell at the P6.p eight-cell stage during the early and mid-L4 stage of development. Expanded gaps in the BM boundary were scored as extending beyond the vulD cell.

[b] Two additional transgenic lines showed similar results.

[c] The *rrf-3* mutant background is more sensitive to somatic RNAi effects.

[d] The cold sensitive mutant *vab-19(e1036)* was scored at 17°C. Wild-type BM gap positioning was normal at this temperature.

ND = not determined; VU = ventral uterine; DU = dorsal uterine